# Controlled self-assembly of gold nanoparticles mediated by novel organic molecular cages

**Wounjhang Park,[1,*] Kazunori Emoto,[1] Yinghua Jin,[2] Akihiro Shimizu,[1] Venkata A. Tamma,[1] and Wei Zhang[2,3]**

[1]*Department of Electrical, Computer & Energy Engineering, University of Colorado, Boulder, CO 80309-0425, USA*
[2]*Department of Chemistry and Biochemistry, University of Colorado, Boulder, CO 80309-0215, USA*
[3]*wei.zhang@colorado.edu*
**won.park@colorado.edu*

**Abstract:** Artificial nanocomposite structures offer a pathway to the development of engineered materials with novel macroscopic properties. Manufacturing the composite materials in a highly efficient yet precise manner remains a challenge and self-assembly of functional nanomaterials offers an attractive solution. In this paper, shape-persistent three-dimensional cage molecules have been used, for the first time, for the self-assembly of gold nanoparticles. The modular construction of cage molecules allows for precise control of inter-particle spacing down to the molecular level. Furthermore, the ability to change the number and flexibility of binding sites provides a means to tune the self-assembly process. We have designed and synthesized two types of cage molecules equipped with different numbers of binding groups with different flexibility. A systematic analysis of the optical and structural characterizations show that the inter-particle spacing within the self-assembled structures are precisely controlled by the choice of the cage molecules. These results highlight that the new self-assembly approach based on molecular cage linkers provides nanometric control over the self-assembled structure.



**OCIS codes:** (160.3918) Metamaterials; (160.4236) Nanomaterials.

## References and links

1. S. H. Park and Y. Xia, "Assembly of Mesoscale particles over large areas and its application in fabricating tunable optical filters," Langmuir **15**(1), 266–273 (1999).
2. P. Jiang, J. F. Bertone, K. S. Hwang, and V. L. Colvin, "Single-crystal colloidal multilayers of controlled thickness," Chem. Mater. **11**(8), 2132–2140 (1999).
3. J. H. Lee, Q. Wu, and W. Park, "Fabrication and optical characterization of gold nanoshell opal," J. Mater. Res. **21**(12), 3215–3221 (2006).
4. S. Kubo, A. Diaz, Y. Tang, T. S. Mayer, I. C. Khoo, and T. E. Mallouk, "Tunability of the refractive index of gold nanoparticle dispersions," Nano Lett. **7**(11), 3418–3423 (2007).
5. J. H. Lee and W. Park, "Three-dimensional metallic photonic crystal based on self-assembled gold nanoshells," Funct. Mater. Lett. **01**(01), 65–69 (2008).
6. J. H. Lee, Q. Wu, and W. Park, "Metal nanocluster metamaterial fabricated by the colloidal self-assembly," Opt. Lett. **34**(4), 443–445 (2009).
7. V. A. Tamma, J. H. Lee, Q. Wu, and W. Park, "Visible frequency magnetic activity in silver nanocluster metamaterial," Appl. Opt. **49**(7), A11–A17 (2010).
8. R. Pratibha, K. Park, I. I. Smalyukh, and W. Park, "Tunable optical metamaterial based on liquid crystal-gold nanosphere composite," Opt. Express **17**(22), 19459–19469 (2009).
9. R. Pratibha, W. Park, and I. I. Smalyukh, "Colloidal gold nanosphere dispersions in smectic liquid crystals and thin nanoparticle-decorated smectic films," J. Appl. Phys. **107**(6), 063511 (2010).
10. S. Y. Park, A. K. R. Lytton-Jean, B. Lee, S. Weigand, G. C. Schatz, and C. A. Mirkin, "DNA-programmable nanoparticle crystallization," Nature **451**(7178), 553–556 (2008).
11. D. Nykypanchuk, M. M. Maye, D. van der Lelie, and O. Gang, "DNA-guided crystallization of colloidal nanoparticles," Nature **451**(7178), 549–552 (2008).
12. Y. Jin, B. A. Voss, R. D. Noble, and W. Zhang, "A shape-persistent organic molecular cage with high selectivity for the adsorption of $CO_2$ over $N_2$," Angew. Chem. Int. Ed. Engl. **49**(36), 6348–6351 (2010).
13. Y. Jin, B. A. Voss, A. Jin, H. Long, R. D. Noble, and W. Zhang, "Highly $CO_2$-selective organic molecular cages: what determines the $CO_2$ selectivity," J. Am. Chem. Soc. **133**(17), 6650–6658 (2011).

#178291 - $15.00 USD Received 19 Oct 2012; revised 28 Nov 2012; accepted 21 Dec 2012; published 9 Jan 2013

14. Y. Jin, B. A. Voss, R. McCaffrey, C. T. Baggett, R. D. Noble, and W. Zhang, "Microwave-assisted syntheses of highly $CO_2$-selective organic cage frameworks (OCFs)," Chem. Sci. **3**(3), 874–877 (2012).
15. C.-X. Zhang, Q. Wang, H. Long, and W. Zhang, "A highly $C_{70}$ selective shape-persistent rectangular prism constructed through one-step alkyne metathesis," J. Am. Chem. Soc. **133**(51), 20995–21001 (2011).
16. C.-X. Zhang, H. Long, and W. Zhang, "A $C_{84}$ selective porphyrin macrocycle with an adaptable cavity constructed through alkyne metathesis," Chem. Commun. (Camb.) **48**(49), 6172–6174 (2012).
17. J. Lohrman, C. Zhang, W. Zhang, and S. Q. Ren, "Semiconducting carbon nanotube and covalent organic polyhedron-$C_{60}$ nanohybrids for light harvesting," Chem. Commun. (Camb.) **48**(67), 8377–8379 (2012).
18. A. Bilić, J. R. Reimers, and N. S. Hush, "Adsorption of pyridine on the gold(111) surface: implications for 'alligator clips' for molecular wires," J. Phys. Chem. B **106**(26), 6740–6747 (2002).
19. S. Y. Quek, M. Kamenetska, M. L. Steigerwald, H. J. Choi, S. G. Louie, M. S. Hybertsen, J. B. Neaton, and L. Venkataraman, "Mechanically controlled binary conductance switching of a single-molecule junction," Nat. Nanotechnol. **4**(4), 230–234 (2009).
20. R. Kaminker, M. Lahav, L. Motiei, M. Vartanian, R. Popovitz-Biro, M. A. Iron, and M. E. van der Boom, "Molecular structure-function relations of the optical properties and dimensions of gold nanoparticle assemblies," Angew. Chem. Int. Ed. Engl. **49**(7), 1218–1221 (2010).
21. W. Zhang and J. S. Moore, "Shape-persistent macrocycles: structures and synthetic approaches from arylene and ethynylene building blocks," Angew. Chem. Int. Ed. Engl. **45**(27), 4416–4439 (2006).
22. A. Yu, Z. Liang, J. Cho, and F. Caruso, "Nanostructured electrochemical sensor based on dense gold nanoparticle films," Nano Lett. **3**(9), 1203–1207 (2003).
23. Y. Joseph, I. Besnard, M. Rosenberger, B. Guse, H.-G. Nothofer, J. M. Wessels, U. Wild, A. Knop-Gericke, D. Su, R. Schlogl, A. Yasuda, and T. Vossmeyer, "Self-assembled gold nanoparticle/ alkanedithiol films: preparation, electron microscopy, XPS-analysis, charge transport, and vapor-sensing properties," J. Phys. Chem. B **107**(30), 7406–7413 (2003).
24. A. Cunningham, S. Mühlig, C. Rockstuhl, and T. Bürgi, "Coupling of plasmon resonances in tunable layered arrays of gold nanoparticles," J. Phys. Chem. C **115**(18), 8955–8960 (2011).
25. C. F. Bohren and D. R. Huffman, *Absorption and Scattering of Light by Small Particles* (Wiley-VCH Verlag GmbH & Co. KgaA, 2004).
26. T. Atay, J.-H. Song, and A. V. Nurmikko, "Strongly interacting plasmon nanoparticle pairs: from dipole-dipole interaction to conductively coupled regime," Nano Lett. **4**(9), 1627–1631 (2004).
27. W. T. Doyle, "Optical properties of a suspension of metal spheres," Phys. Rev. B Condens. Matter **39**(14), 9852–9858 (1989).
28. V. Yannopapas and A. Moroz, "Negative refractive index metamaterials from inherently non-magnetic materials for deep infrared to terahertz frequency ranges," J. Phys. Condens. Matter **17**(25), 3717–3734 (2005).
29. J. C. M. Garnett, "Colours in metal glasses and in metallic films," Philos. Trans. R. Soc. Lond. A **203**(359-371), 385–420 (1904).
30. P. B. Johnson and R. W. Christy, "Optical constants of the noble metals," Phys. Rev. B **6**(12), 4370–4379 (1972).
31. See, for example, G. W. Milton, *Theory of Composites* (Cambridge University Press, 2004).
32. B. Abeles and J. I. Gittleman, "Composite material films: optical properties and applications," Appl. Opt. **15**(10), 2328–2332 (1976).
33. V. Yannopapas, A. Modinos, and N. Stefanou, "Optical properties of metallodielectric photonic crystals," Phys. Rev. B **60**(8), 5359–5365 (1999).
34. N. Stefanou, V. Karathanos, and A. Modinos, "Scattering of electromagnetic waves by periodic structures," J. Phys. Condens. Matter **4**(36), 7389–7400 (1992).
35. N. Stefanou, V. Yannopapas, and A. Modinos, "MULTEM 2: a new version of the program for transmission and band-structure calculations of photonic crystals," Comput. Phys. Commun. **132**(1-2), 189–196 (2000).
36. A. Moroz and C. Sommers, "Photonic band gaps of three-dimensional face-centered cubic lattices," J. Phys. Condens. Matter **11**(4), 997–1008 (1999).
37. V. Yannopapas, "Effective-medium description of disordered photonic alloys," J. Opt. Soc. Am. B **23**(7), 1414–1419 (2006).

## 1. Introduction

Artificial structured materials such as photonic crystal and metamaterial hold high promise of providing a path to by-design optical materials with engineered optical properties. In the past decade, the field has seen an explosive growth fuelled by the demonstrations of novel properties like negative refractive index and invisibility. One of the major roadblocks for practical applications is the lack of efficient fabrication technology, which is also one of the grand challenges in nanotechnology in general. So far, vast majority of optical metamaterials have been fabricated by top-down techniques such as electron-beam lithography or focused ion beam milling. While these techniques provide powerful means to sculpt nanostructures with high precision, they are slow, expensive and generally limited to two-dimensional structures. An efficient and scalable technique capable of producing large-area, three-dimensional (3D) structures is critically needed and self-assembly of nanoparticles offers an attractive solution to this problem.

#178291 - $15.00 USD Received 19 Oct 2012; revised 28 Nov 2012; accepted 21 Dec 2012; published 9 Jan 2013

The simplest approach of self-assembling nanoparticles is to use hard sphere interaction. When the nanoparticles are highly monodispersed, the hard sphere interaction could lead to close-packing of nanoparticles into the face centered cubic structure [1]. Controlled drying of solvent could be used for close-packing of monodispersed nanoparticles, too [2]. While these methods provide simple and effective ways to obtain large-size, 3D ordered structures, they generally produce high density of defects and long-range order has yet to be achieved by these techniques. Furthermore, self-assembly of plasmonic nanoparticles presents an additional challenge. It is often the case that the plasmonic nanoparticle volume fraction has to be on the order of 1~10% to observe interesting optical phenomena. However, such high concentration is very difficult to achieve due to the strong van der Waals interaction between metal nanoparticles, which tends to lead to irreversible agglomeration [3]. In a typical organic solvent, maximum achievable volume fraction of gold nanoparticles is less than 0.1% [4], while many novel phenomena in metamaterials and photonic crystals typically require much higher volume fraction. It is therefore necessary to find a way to overcome the short-range van der Waals force. One way is to increase the electrostatic repulsion to counter the van der Waals force [5]. This can be accomplished by coating the particle surface with electrically charged molecules. Alternatively, one can incorporate thin coatings that provide strong steric hindrance. Recently, we accomplished successful self-assembly of gold and silver nanoparticles using template-directed self-assembly [6,7]. In this approach, nano-template is first fabricated by laser interference lithography, which is capable of generating highly ordered nanoscale patterns over centimeter-scale size. The nano-patterns on the template are chosen to produce desired electric or magnetic responses. Gold and silver nanoparticles are then self-assembled to fill the nano-patterns on the template, producing self-assembled metamaterial structures which exhibited electric and magnetic resonances as designed. However, the self-assembled nanoparticle clusters showed up to ~18% variations in the cluster size due primarily to the colloidal instability persistent in the system even after the inert coatings.

Although the template-directed self-assembly produced promising results, it would generally be desirable to do away with template. One way to accomplish template-free self-assembly of nanoparticles with high metal fraction is to use liquid crystal matrix in which soft matter interaction can provide stabilizing mechanisms. A recent work on gold nanoparticle dispersion in smectic A liquid crystal matrix showed that highly uniform and stable dispersion of gold nanoparticles was possible even at extremely high volume fractions (up to 50%) [8]. In this system, the strong curvature in molecular alignment created by the presence of nanoparticles produces repulsive force between the nanoparticles strong enough to overcome the van der Waals attractive force, in a remarkably similar mechanism for the stable dislocation known to be present in smectic A liquid crystals [9]. Yet another direction to accomplish highly controlled self-assembly of nanoparticles is to use binding molecules grafted on the nanoparticles. In contrast to the template-directed self-assembly and liquid crystal based self-assembly, both of which rely on physical interactions between particles and template or matrix, this approach takes advantage of chemical interactions between the binding molecules, potentially providing much greater degree of control in the self-assembly process. One of the most widely studied molecules is DNA which offers a programmable sequence-based interaction mechanism [10,11]. It is undoubtedly a powerful technique but it still faces many challenges with regards to achieving scalability, functionality and complexity.

In this paper, we report a new approach to plasmonic nanoparticle self-assembly based on 3D shape-persistent cage molecules. Well-defined, rigid, 3D purely organic cage-like molecules have attracted great research attention due to their unique shape-persistency, structure-tunability, and chemical and thermal stability. These molecular cages have been utilized in various fields, such as carbon capture [12–14], fullerene separation [15,16], light harvesting [17], etc. However, to the best of our knowledge, utilizing rigid cage molecules as linkers to control the nanoparticle assembly has not yet been explored. Recent significant progress in the development of dynamic covalent chemistry (DCC) enables the highly efficient synthesis of cage compounds in a modular fashion. The modular construction of cage

#178291 - $15.00 USD Received 19 Oct 2012; revised 28 Nov 2012; accepted 21 Dec 2012; published 9 Jan 2013

molecules provides the design flexibility required to control the nanoparticle assembly process. Also, the shape-persistent nature of the molecules leads to highly stable and robust structures. In the following, we report successful self-assembly of gold nanoparticles using two different types of cage molecules as linkers. Our results shed light on how the molecular structures affect and thus can be used to control the self-assembly process.

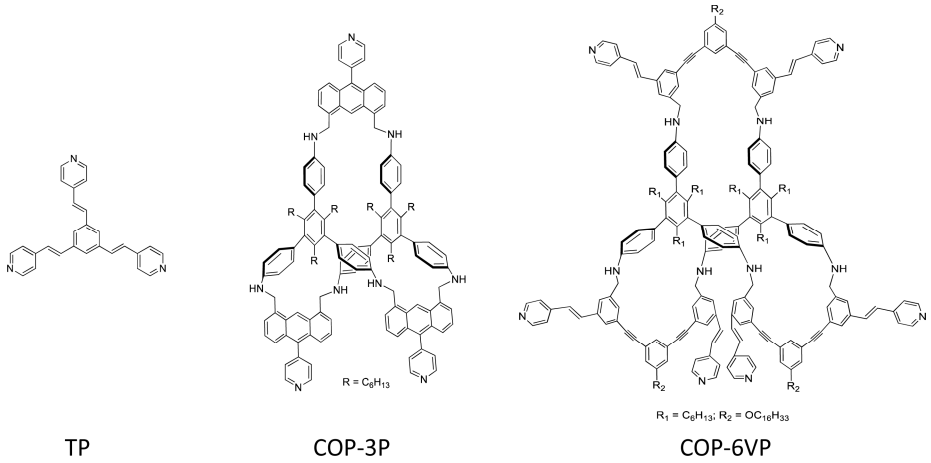


Fig. 1. Schematic diagrams of molecules used for self-assembly of gold nanoparticles.

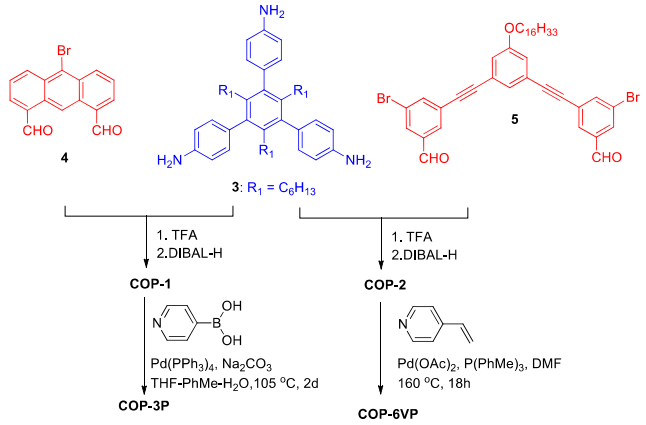


Fig. 2. Synthesis of **COP-3P** and **COP-6VP** (see Media 1).

## 2. Cage molecule synthesis and self-assembly

We designed, synthesized and investigated two different cage molecules, also called covalent organic polyhedrons (COP), tri(4-pyridyl)-substituted COP (**COP-3P**) and hexa(4-pyridylvinyl)-substituted COP (**COP-6VP**) along with a small ligand molecule, 1,3,5-tri(4-pyridylvinyl)benzene (**TP**), which was used as a reference compound. These molecules were chosen to provide insights into how the binding efficiency and kinetics are influenced by the cage structures on the molecular-level. As shown in Fig. 1, pyridyl groups were installed on all three molecules as anchoring sites for binding with gold nanoparticles. The binding between gold and pyridyl group is well characterized and widely used in many applications [18–20]. **TP** and **COP-3P** have three pyridyl groups whereas **COP-6VP** has six. Conventionally, the organic cage compounds are prepared through kinetically controlled, irreversible coupling reactions, which generally provide cage products in very low yield due to the intrinsic "over-shooting" problem [21]. However, recent advances in dynamic covalent

#178291 - $15.00 USD Received 19 Oct 2012; revised 28 Nov 2012; accepted 21 Dec 2012; published 9 Jan 2013

chemistry have enabled facile access to nanometer-sized covalently linked cage molecules from simple synthetic precursors [12,15]. As shown in Fig. 2, trigonal prismatic cage **COP-1** and **COP-2** were constructed through dynamic imine metathesis, in which the product formation was under thermodynamic control, from 2:3 equivalent of triamine and dialdehyde building units. Bromo functional groups were installed on each of the side arms as the synthetic handle for further introducing the nanoparticle binding sites (Details in Media 1). The pyridine binding sites were then installed through cross-coupling reaction of **COP-1** and **COP-2** with pyridine-4-boronic acid and 4-vinylpyridine respectively to provide **COP-3P** and **COP-6VP**.

Thanks to its small size (14.7Å), **TP** molecules can readily rotate and reorient themselves and thus bind with gold nanoparticles efficiently [20]. The COP molecules are larger and therefore not as nimble as **TP**. This difference was obvious when the gold nanoparticle solution and cage molecule solution were mixed for a quick test of binding kinetics. The original gold nanoparticle solution with an average particle size of 14 nm was red due to the strong surface plasmon absorption peak at 520 nm. When **TP** was added, the solution immediately turned purple. The optical extinction spectrum revealed the emergence of a second peak near 700 nm, which was due to the coupling between individual nanoparticle plasmon resonances. This observation was consistent with a previous report [20] and was a direct evidence of nanoparticle cluster formation and suggests highly efficient binding between **TP** ligand molecules and gold nanoparticles. For both **COP-3P** and **COP-6VP**, the solution color change occurred slowly over an hour or longer, indicating the nanoparticle assembly was much slower. Furthermore, in contrast to **TP**, mixing gold nanoparticles with **COP-3P** or **COP-6VP**, only led to a slight red shift of absorption peak without showing the second peak near 700 nm on the UV-Vis spectrum (Fig. S1 in Media 1). These results were consistent with those from self-assembly and the mechanism behind this phenomenon is elucidated later.

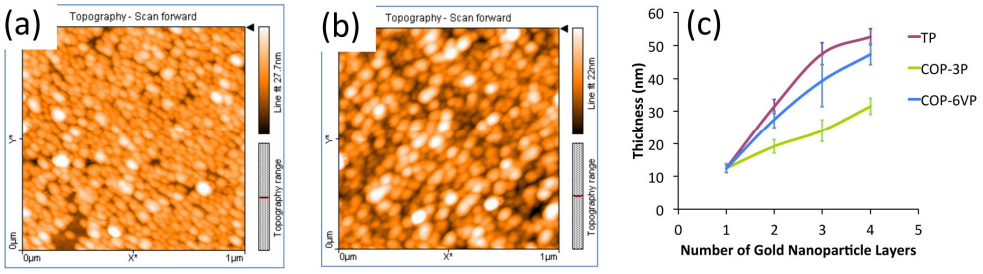


Fig. 3. Topography scans obtained by AFM for (a) monolayer of gold nanoparticles and (b) 4 layers of gold nanoparticles self-assembled by **COP-3P** molecules. (c) Thickness measured by AFM as a function of the number of gold nanoparticle layers for self-assembly mediated by various molecules.

Self-assembly of gold nanoparticles were conducted in a layer-by-layer fashion similarly to what have been reported previously [22,23]. In this process, the first layer of gold nanoparticles on the substrate was formed by electrostatic interaction between the negatively charged gold nanoparticles in aqueous solution and the substrate surface positively charged by amine-functionalization. Atomic force microscopy (AFM) showed that a monolayer of high-density, well-dispersed gold nanoparticle was formed (Fig. 3(a)). The particle surface density was measured to be ~730 $\mu m^{-2}$, which was comparable to what has recently been reported for gold nanoparticle deposition via electrostatic interaction [24]. Due to the finite size of the AFM tip, the individual nanoparticle size in AFM images was 31 nm. The average center-to-center spacing between two neighboring nanoparticles was 37 nm. On top of the monolayer prepared this way, cage molecule solution and gold nanoparticle solution were applied sequentially by drop-casting method. The concentration and duration of deposition of each layer were chosen to ensure saturated surface coverage of linker molecules (Details in Media 2). After each cycle of sequential application of cage molecule solution and gold nanoparticle

#178291 - $15.00 USD Received 19 Oct 2012; revised 28 Nov 2012; accepted 21 Dec 2012; published 9 Jan 2013

solution to the self-assembly surface, the surface topography and layer thickness were measured by AFM. The AFM images generally showed a surface with well dispersed gold nanoparticles, as shown in the example of 4 layer gold nanoparticles self-assembled with **COP-3P** molecules in Fig. 3(b). Although not shown, the surfaces of **TP** and **COP-6VP** mediated self-assembly exhibited similar topographies. As the number of layers of self-assembled nanoparticles was increased, the average particle size increased to 45~55 nm in diameter, indicating a small degree of clustering of nanoparticles on the self-assembly surface. However, the rms roughness remained small and lied between 3 and 6 nm in all samples, indicating uniform layer-by-layer assembly was accomplished. Particle surface density also remained stable between 800 and 1000 $\mu m^{-2}$.

To determine whether the gold nanoparticle layers were indeed assembled in layer-by-layer fashion, thickness was measured by AFM as the self-assembly was being carried out. As shown in Fig. 3(c), the total gold nanoparticle layer thickness increased in all cases as more cycles of self-assembly were conducted, indicating that the gold nanoparticles were captured and bound to the growth surface by the linker molecules used for self-assembly. However, the thickness was substantially lower for the samples self-assembled with **COP-3P** molecules than other molecules. This was attributed to the inefficient binding between **COP-3P** and gold nanoparticles, which was expected from the molecular structure of **COP-3P**. As shown in Fig. 1, **COP-3P** had pyridyl binding groups rigidly attached to the cage frame. In contrast, **COP-6VP** had more flexible vinyl groups (through vinyl and phenyl C-C single bond rotation) linking the pyridyls to the cage frame, thereby providing rotational freedom to the binding groups. As a result, **TP** and **COP-6VP** molecules with flexible binding groups could bind much more efficiently with gold nanoparticles than **COP-3P** molecule. In the thickness data, the inefficient binding of **COP-3P** with gold nanoparticles manifested itself with lower thicknesses. For the other two molecules, **TP** and **COP-6VP**, the thicknesses were similar. The differences in thicknesses were 5~8 nm, which was substantially smaller than the single gold nanoparticle size, 14 nm. It could thus be stated that highly efficient binding with gold nanoparticles was achieved in both cases. While the thickness differences were small, the thickness was consistently larger with **TP** than **COP-6VP**. This result showed that there was some correlation between the molecule size and binding efficiency. **TP** was the smallest planar molecule and thus able to readily diffuse, rotate and reorient itself to bind with gold nanoparticles. This allowed high accessibility of ligand group to nanoparticles, leading to a denser nanoparticle array on the surface. The larger size **COP-6VP** molecule was not as nimble as **TP** and consequently exhibited less efficient binding, which resulted in lower thicknesses than **TP**. However, despite the substantially larger size, **COP-6VP** resulted in thicknesses only slightly smaller than **TP**. This was because **COP-6VP** had a larger number (six) of binding groups than **TP** which had three.

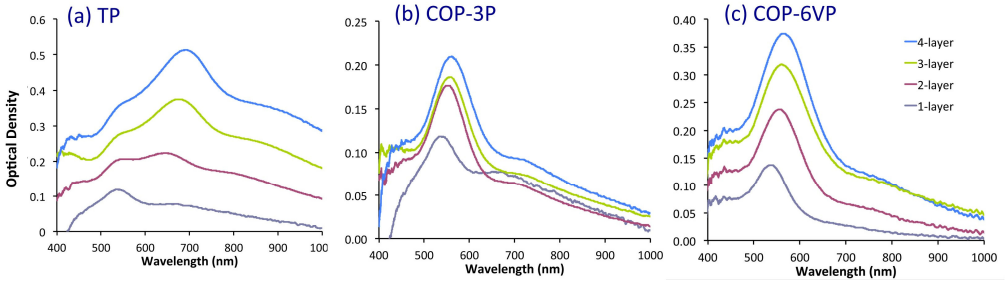


Fig. 4. Optical extinction spectra for self-assembled gold nanoparticles using linker molecules (a) **TP**, (b) **COP-3P** and (c) **COP-6VP**.

## 3. Optical characterizations and analysis

Optical extinction spectroscopy was carried out for the self-assembled layers of gold nanoparticles. Figure 4 show the extinction spectra of 1~4 layers of gold nanoparticles self-

#178291 - $15.00 USD Received 19 Oct 2012; revised 28 Nov 2012; accepted 21 Dec 2012; published 9 Jan 2013

assembled with **TP**, **COP-3P**, and **COP-6VP** molecules. In all cases, the extinction increased as more layers were assembled. This was consistent with the thickness data which showed the thickness increased with increasing number of self-assembled layers with all three molecules. However, the peak extinction values showed significant differences depending on which molecule was used for self-assembly. **TP** resulted in the highest extinction and **COP-3P** gave the lowest with **COP-6VP** showing slightly lower extinction than **TP**. Since none of the linker molecules has absorption above 400 nm, the optical extinction in the visible spectrum should be proportional to the total number of gold nanoparticles present in the light path, which in our samples is determined by the thickness of the self-assembled layer and density of gold nanoparticles in it. The peak extinction observed in **TP**, **COP-3P** and **COP-6VP** samples was in excellent agreement with the thickness data obtained by AFM, once again confirming that **TP** led to the most efficient binding followed by **COP-6VP** and **COP-3P** in that order.

The optical extinction spectra offer another information on gold nanoparticle packing from the position of peak extinction. The origin of the extinction peak is obviously the surface plasmon resonance of gold nanoparticles. According to the Mie theory [25], a 14 nm size gold sphere placed on a glass substrate should exhibit extinction peak at around 530 nm, which was exactly what was observed from the monolayer samples as shown in Fig. 4. This confirms that the gold nanoparticles are uniformly distributed on the surface with minimal aggregations. As more gold nanoparticle layers were added by subsequent self-assembly processes, the surface plasmon resonances of individual gold nanoparticles couple together with those of neighboring nanoparticles and the resultant delocalization consequently leads to the lowering of resonance frequency and red shift in the optical extinction peak. The peak shift depends on the inter-particle spacing. The closer the nanoparticles are, the stronger the coupling between the neighboring particles is and thus the larger the red shift in optical spectrum. This is a well-known behavior that has been observed in dimers [26] and is also consistent with the effective medium analysis presented later. In the optical extinction spectra presented in Fig. 4, **TP** shows by far the largest red shift. In fact, the **TP** spectra in Fig. 4(a) show that the original extinction peak at 530 nm which was dominant in the monolayer sample became overwhelmed by the fast emerging second peak at a longer wavelength. The position of the second peak exhibited a modest red shift from 640 nm for 2 layer sample to 685 nm for 4 layer sample. In contrast, the **COP-3P** spectra in Fig. 4(b) show a very small red shift with increasing number of layers to 550 nm for the 4 layer sample. In the **COP-6VP** spectra, the red shift was slightly larger, reaching 560 nm for the 4 layer sample, as shown in Fig. 4(c). These observation led us to conclude that the self-assembly with **TP** resulted in the most dense packing of gold nanoparticles with smallest inter-particle spacing, **COP-3P** produced the lowest density gold nanoparticle assembly, and **COP-6VP** slightly higher packing density.

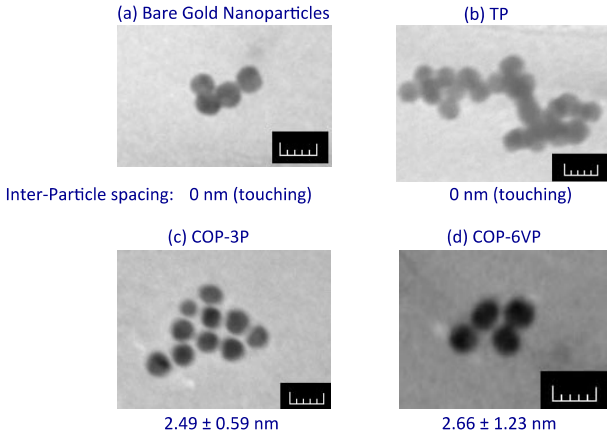


Fig. 5. Transmission electron micrographs of gold nanoparticle clusters with various linker molecules: (a) bare nanoparticles, (b) **TP**, (c) **COP-3P** and (d) **COP-6VP**. The scale bars indicate 20 nm.

#178291 - $15.00 USD Received 19 Oct 2012; revised 28 Nov 2012; accepted 21 Dec 2012; published 9 Jan 2013

For more quantitative analysis, the extended Maxwell Garnett effective medium theory [27,28] was used to fit the optical extinction spectra. In this method, the polarizability of individual gold nanoparticle was first calculated by using the Mie theory and then the Maxwell Garnett mixing rule [29] was used to calculate the complex effective refractive index for the composite structure. It has been shown that the extended Maxwell Garnett effective medium theory provides adequate descriptions of metal nanoparticle clusters by comparing with the rigorous numerical modeling by the multiple scattering method [7]. In order to apply the extended Maxwell Garnett theory, we need to know the gold nanoparticle size, their density inside the self-assembled film and the refractive indexes of gold and the background medium. The average size of the gold nanoparticle was measured to be 14 nm by the scanning electron micrographs (SEMs). The average spacing between the nanoparticles is determined by the cage molecule and was directly measured by a series of transmission electron micrographs (TEMs). As shown in Fig. 5, the TEM images clearly showed the inter-particle spacing was related to the cage molecules used. The bare nanoparticles and **TP**-grafted nanoparticles formed clusters of touching nanoparticles whereas the cage molecule coated nanoparticles clearly showed finite gaps between them. The average spacing between the adjacent nanoparticles was determined by averaging 30~40 inter-particle spacings extracted from a series of TEM images. For **COP-3P**, the gap was measured to be 2.49 ± 0.59 nm and for **COP-6VP** it was 2.66 ± 1.23 nm. These values are in excellent agreement with the cage molecule sizes. From the molecular structure, the transverse size of **COP-3P** defined as the distance between adjacent binding sites was estimated to be 2.73 nm. For **COP-6VP**, since there were six binding sites, the distance between a pair of biding sites varied from 1.5 nm to 3.5 nm. Therefore, the slightly larger average gap size together with larger standard deviation obtained for **COP-6VP** was considered consistent with the molecular structure. We also note that planar linker molecules similar to **TP** were shown to result in touching nanoparticles [20]. We therefore infer that the 3D structure of cage molecules is an important factor in creating finite spacing between nanoparticles.

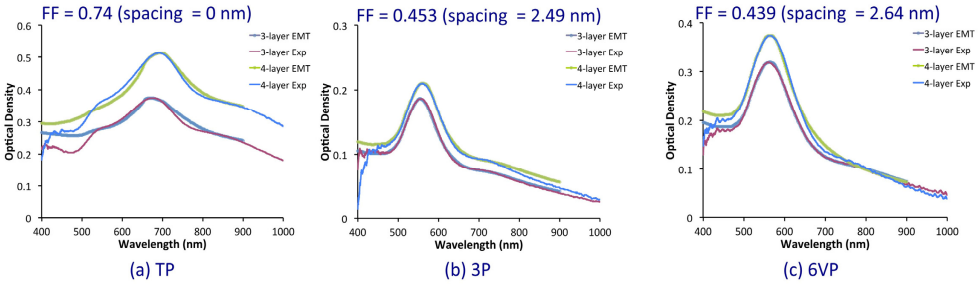


Fig. 6. Experimental optical extinction spectra and the effective medium theory fitting for 3-layer and 4-layer self-assembled gold nanoparticle films using (a) **TP**, (b) **COP-3P** and (c) **COP-6VP** (see Media 2).

For the refractive index of gold, we used the experimentally measured dielectric function [30] with slightly increased imaginary part to account for higher loss due to increased scattering in nanoscale geometry as customarily done in plasmonic nanostructure research. The background medium refers to the space between gold nanoparticles and is composed of cage molecules and air. It was not possible to accurately determine the amount of cage molecules in the space between gold nanoparticles. We therefore measured the refractive index of cage molecule thin films by ellipsometry (data provided in the Media 2) and then used the volume fraction of cage molecules in the background medium as a fitting parameter to fit the experimentally measured optical extinction spectra. In all 6 cases presented in Fig. 6, we were able to obtain excellent fitting with cage molecule volume fraction of 0.4~0.5 in the background medium. We also note that the metamaterial structures self-assembled with **COP-3P** and **COP-6VP** molecules exhibited a small feature in the long wavelength region between 700 and 800 nm. This was attributed to the formation of larger clusters of gold nanoparticles

#178291 - $15.00 USD Received 19 Oct 2012; revised 28 Nov 2012; accepted 21 Dec 2012; published 9 Jan 2013

during the drying process introduced between application of cage molecule solution and gold nanoparticle solution. When we kept the samples wet at all times, this long wavelength feature disappeared.

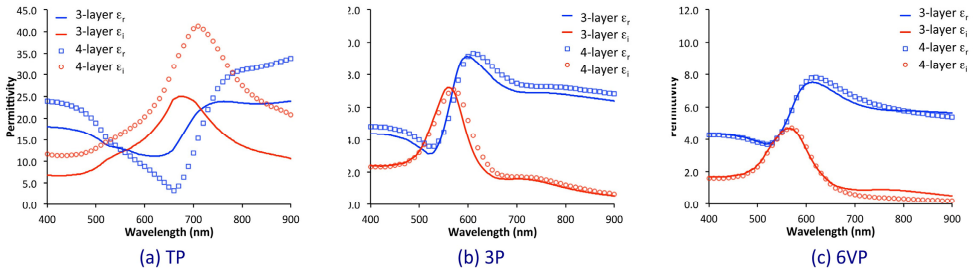


Fig. 7. Real ($\varepsilon_r$) and imaginary ($\varepsilon_i$) parts of permittivity extracted from the effective medium theory fitting presented in Fig. 6. 3-layer samples are plotted with solid lines and 4-layer samples were plotted with symbols.

From the fitting by the effective medium theory presented in Fig. 6, effective permittivity can be extracted. The real and imaginary parts of effective permittivity are plotted in Fig. 7. The general features of the effective permittivity were similar in all three cases and in agreement with the classical oscillator model in that the imaginary part exhibited a peak corresponding to the absorption band observed in experiments while the real part showed a wiggle around the resonance. The origin of the resonance is obviously the surface plasmon resonance of individual gold nanoparticles shifted and broadened through the dipole-dipole interaction taken into account in the extended Maxwell Garnett effective medium theory. While the general behavior was the same for all three samples, a key difference was observed between **TP** and the two cage molecules. The two samples prepared with **COP-3P** and **COP-6VP** showed almost identical dielectric functions for the 3-layer and 4-layer cases while there were large discrepancies in **TP**. Ideally, the same dielectric function should be retrieved irrespective of the sample thickness if the effective medium theory is truly valid. The validity of various effective medium theories has a long history of debate and is well documented [31]. Maxwell Garnett theory or extended Maxwell Garnett theory are generally considered better suited than other approaches such as Bruggeman theory, for the particulate composites as those discussed in this paper [32,33]. Rigorously speaking, the Maxwell Garnett theory should be valid only in the small particle size and small volume fraction limit. However, for small particles, it was shown to be reasonably accurate over a surprising wide range of volume fraction [7]. This was once again confirmed by the present study. In the cases of **COP-3P** and **COP-6VP** samples, the fact that almost identical dielectric functions were retrieved for two different thicknesses suggested that meaningful dielectric functions were obtained. The differences between 3-layer and 4-layer cases were only a few percent at most wavelengths and less than 10% even at maximum. The small differences most likely stemmed from the small difference in the background index used to obtain the best fit to the experimental extinction spectra. Since the background index depends on the volume fraction of cage molecules within the gap space between the gold nanoparticles, it is perfectly understandable that there could exist small variations from sample to sample. The large discrepancies between the 3-layer and 4-layer dielectric functions obtained for **TP**, however, indicated the failure of the Maxwell Garnett effective medium theory. This was in fact expected because the Maxwell Garnett theory assumes particulate inclusions in a host medium and is well known to fail to provide the same result when the inclusion and host media are interchanged. Therefore, when the composite structure exhibits an interconnected network topology such as the one exhibited by the touching gold nanoparticles in **TP** samples, the Maxwell Garnett theory is not suitable. This was confirmed by the failure to obtain the same dielectric function for both the 3-layer and 4-layer samples self-assembled by **TP**. If the sample were composed of air "particles" in gold matrix, it would have been possible to use Maxwell Garnett theory by calculating the polarizability of air spheres in gold. However, in

#178291 - $15.00 USD Received 19 Oct 2012; revised 28 Nov 2012; accepted 21 Dec 2012; published 9 Jan 2013

the present case, both gold and air were expected to exhibit network topology and thus the Maxwell Garnett approach was considered simply not applicable.

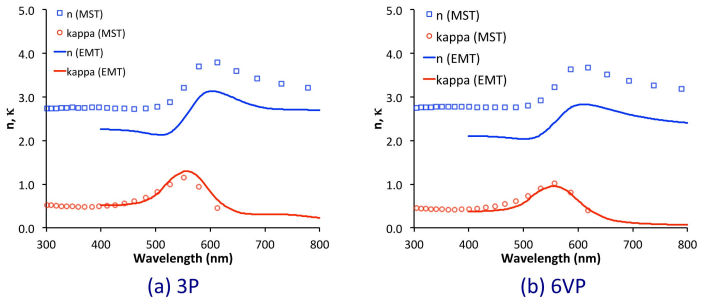


Fig. 8. Real (n) and imaginary (κ) parts of refractive index calculated from the effective medium theory (solid lines) and the multiple scattering theory (symbols) for the 4-layer samples prepared with (a) **COP-3P** and (b) **COP-6VP**.

As further evidence that the retrieved dielectric functions for **COP-3P** and **COP-6VP** samples are meaningful, we conducted numerical simulations using the multiple scattering theory [34,35]. This is a rigorous approach without any approximation, other than the fact that the spherical wave expansion used to calculate the multiple scattering between spherical inclusions has to be terminated at a finite number, and is therefore a good test for the validity of effective medium approximation. Since the multiple scattering calculation provides the photonic band structure, or the ω-k relationship, we can extract the refractive index from it and compare with the refractive indexes calculated from the effective permittivity given in Fig. 7. The real and imaginary parts of the refractive index calculated by the multiple scattering theory and effective medium theory are shown in Fig. 8. The extinction coefficient, κ, showed excellent agreement for both **COP-3P** and **COP-6VP** samples. For the real part of the refractive index, the effective medium results were slightly smaller than the multiple scattering results but the spectral features such as the wavelengths of local maximum and minimum were in excellent agreement. There are two possible reasons for the observed differences. First, the Maxwell Garnett theory was known to underestimate the effective refractive index compared to the rigorous multiple scattering theory [36]. Additionally, the multiple scattering theory assumed perfectly periodic structures whereas the real structures used for experiments and subsequently for fitting by the effective medium theory are random composites. In our calculations, we assumed face-centered cubic arrangements of gold nanoparticles with inter-particle spacing of 2.49 nm for **COP-3P** and 2.64 nm for **COP-6VP** samples, as determined by the TEM images. It is therefore naturally expected that the multiple scattering results would not precisely predict the experimental data. The degree of disagreement would depend on various aspects of the composite structure. In a study of disordered silicon-air photonic crystal structures, Yannopapas showed that the discrepancies in effective permittivity become more significant for large volume fractions and also for large dielectric contrast between the spheres and background medium [37]. For silicon spheres in air, the difference of effective permittivity between ordered and disordered structures reached ~15% for volume fractions comparable to our systems. Given that gold nanoparticle would even more strongly interact with light due to surface plasmon resonance, the observed difference of 20~25% in refractive index between the multiple scattering theory and effective medium theory is considered reasonable. Finally, we did not conduct multiple scattering calculations for the **TP** samples because the numerical instability prevented us from simulating touching spheres and also because the validity of effective medium description itself was in question as discussed before.

The main result reported in this paper is the fact that the experimentally measured optical extinction spectra could be fitted very well with the effective medium theory using the inter-particle spacing measured by TEM. The subsequent discussions further showed that the effective medium results were reliable. From this, we could conclude that we were able to

#178291 - $15.00 USD Received 19 Oct 2012; revised 28 Nov 2012; accepted 21 Dec 2012; published 9 Jan 2013

accurately control the inter-particle spacing in the self-assembled film by the choice of cage molecules. Inter-particle spacing is a critical parameter that dictates the coupling between the plasmon resonances and thus ultimately determines the effective dielectric function of the self-assembled structure. The capability of controlling the inter-particle spacing down to the nanometer scale affords us the ability to finely control the dielectric function of the self-assembled artificial structured materials.

## 4. Conclusions

We report the first experimental demonstration of nanoparticle self-assembly enabled by shape-persistent 3D cage molecules. The modular construction of cage molecules allows for a precise control of inter-particle spacing down to the molecular level. Furthermore, the ability to change the number and flexibility of binding sites provides a means to tune the self-assembly process. We have synthesized two different types of cage molecules to demonstrate successful self-assembly of gold nanoparticles. The experimentally observed self-assembly dynamics were consistent with the expectations from the molecular structures. A systematic and thorough analysis of the optical and structural characterization results showed that high-quality self-assembled metamaterial structures were obtained and their optical properties were explained well by the effective medium theory. The effective medium theory allowed us to conclude the inter-particle spacing in the self-assembled metamaterial structure was precisely controlled by the size of the cage molecule used in self-assembly. The shape-persistent 3D cage molecules represent a new class of linker molecules that could enable mechanically stable and robust assembly. The high flexibility in molecular design and ability to contain functional nanoparticles inside the molecular cavity hold high promise of enabling novel self-assembled structures with precise control. As the first step in that direction, this paper showed that the new self-assembly approach based on molecular cages could provide nanometric control over the self-assembled structure.

## Acknowledgment

This work was supported by the DARPA COMPASS program through a grant from DOI NBC (N11AP20027) and ARO grant W911NF-12-1-0581.

#178291 - $15.00 USD Received 19 Oct 2012; revised 28 Nov 2012; accepted 21 Dec 2012; published 9 Jan 2013